Chapter 5

Fluid Flow, Brecciation, and Shear Heating on Faults: Insights from Carbonate Clumped-Isotope Thermometry

Erika Swanson, Brian Wernicke, and John Eiler

Division of Geological and Planetary Sciences

California Institute of Technology

Pasadena, CA 91125

For submission to Tectonics

ABSTRACT

The Mormon Peak and Heart Mountain detachments are carbonate-hosted low-angle faults of Tertiary age in the western United States that formed in the uppermost continental crust. Both faults were active during regional explosive volcanism, with a magmatic center of approximately 30 km distant in the case of the Mormon Peak detachment, and directly within the area of exposure of the Heart Mountain detachment. We present results from 137 carbonate clumped-isotope thermometric analyses within fault rocks related to the Mormon Peak and Heart Mountain detachments. We collected breccias, veins, gouges, and other fault rocks predominantly from within ~1 meter of the detachments. Our results suggest the breccias and gouges are mixtures of (1) host rock, (2) authigenic or vein material, and (3) in some cases includes material that is frictionally heated during faulting. The majority of fault rocks are depleted in $\delta^{18}O$ and cold relative to the host rock, indicating the addition of material that precipitated from meteoric water under ambient conditions. However, a few samples preserve temperatures of over 250 °C, which based on textural and geochemical criteria are difficult to explain other than by frictional heating during slip. The primary contrast between the two faults is the greater variation and higher ambient temperatures associated with the Mormon Peak detachment (c. 25 to 165 °C), and evidence for circulation of meteoric fluids up the fault plane from depths of at least 4 km. Surprisingly, despite its much closer association with magmatism, ambient temperatures along the Heart Mountain detachment are general lower and show much less variation (40-90 °C). In both

cases magmatic fluids appear to have played a very minor role, if any, in the carbonate isotopic signature.

INTRODUCTION

The classic Andersonian theory of fault mechanics presumes that the earth obeys Coulombic failure criteria, and that one of the principal stress axes is normal to the earth's surface. Under these conditions, the ratio of shear stress to normal stress on low-angle normal faults (<30 °) is too low for both fracture initiation and continued slip, even if the ambient pore fluid pressure is lithostatic (e.g. Axen, 2004). The ubiquity of normal faults that both formed and slipped at low angle (e.g. Pierce, 1980; Mount and Suppe, 1987; Lister and Davis, 1989; Scott and Lister, 1992; Wernicke, 1995; Livaccari et al., 2001; Morley, 2014) has accordingly led to extensive theoretical, experimental and field research into this enduring enigma, resulting in explanations that emphasize some form of fluid-assisted weakening of fault zone materials, rotation of stress axes, or both (e.g., Yin, 1989; Melosh, 1990; Axen, 1992; Parsons and Thompson, 1993; Lister and Baldwin, 1993; Forsyth, 1993; Zoback and Townend, 2001; Bos and Spiers, 2001; Collettini and Holdsworth, 2004). The same puzzle arises in the case of major strike-slip faults such as the San Andreas, which also appears to be oriented nearly perpendicular to the maximum principal stress direction in the upper crust (e.g. Mount and Suppe, 1987; Rice, 1990; Hickman and Zoback, 2004; Lockner et al., 2011). It is therefore generally acknowledged that the lack of resolution of this "stress paradox" remains the primary hurdle in understanding the mechanics of faulting.

Fluid-assisted weakening mechanisms generally invoke high temperatures, due to (1) friction, up to and including melting in silicate rocks (e.g. Sibson 1975 ; Cowan 1999; Hirose and Shimamoto, 2005), or decarbonation in carbonate rocks (e.g. Sulem and Famin, 2009; Han et al, 2010); or (2) magmatism, including the injection of volcanic gases (Hughes, 1970) and pressurization via magmatic heating of pore waters (Aharanov et al., 2006). Weakening may thus occur by reducing the coefficient of friction (as appears to be the case for the San Andreas fault at shallow depth; Lockner et al., 2011), or by the development of near-lithostatic overpressure confined to the slip zone (e.g. Rice, 2006; DePaola et al., 2011).

In this paper, we investigate the extent to which these mechanisms might apply to natural faults by using carbonate clumped-isotope thermometry on fault rocks and vein systems to track the origin and thermal evolution of fault zone fluids. In order to apply this technique to fault systems, we have focused on two carbonate-hosted, upper crustal low-angle faults, including the Heart Mountain detachment in the Absaroka Range and environs in NW Wyoming, and the Mormon Peak detachment in the Mormon Mountains in SE Nevada. Both faults are well exposed over areas of c. 1000 km^2, and have displacements of at least 10 km. Because both faults primarily involve lower Paleozoic dolomitic strata in in platform or cratonic settings, their stable isotope composition is quite heavy in both oxygen (c. +20-25 ‰ VSMOW) and carbon (c. 0-4 ‰ VPDB), so that exchange phenomena with relatively light meteoric water and magmatic fluids can be expected to yield robust signals. Accordingly, each of the two areas has an extensive history of investigation both structurally and isotopically (for Heart Mountain, Pierce, 1980; Hauge, 1985, 1990; Templeton et al., 1995; Douglas et al., 2003; Anders et al., 2010; for the Mormon Mountains, Wernicke et al., 1985; Losh, 1997; Anders et al., 2006; Walker, 2007; Anderson et al., 2010; Diehl et al., 2010; Swanson et al., 2012). Both the Heart Mountain and Mormon Peak detachments developed synchronously with regional magmatism, the former during development of the Eocene Absaroka Volcanic Supergroup (c. 52-48 Ma; Smedes and Prostka, 1972; Feeley and Cosca, 2003), and the latter during the development of the Miocene Kane Springs Wash caldera (c. 15-14 Ma; Scott et al., 1995).

The faults exhibit two key distinctions in their mode of origin that bear on the interpretation of thermometric data, including (1) their proximity to coeval magmatic centers and (2) their depth of development. The Heart Mountain detachment and allochthon are generally regarded as resulting from the gravitational collapse of a magmatic center (Sunlight Volcano and related units), with the detachment initiating at a depth of 1000-2000 m (Beutner and Hauge, 2009, and references therein). In contrast, the Mormon Peak detachment and allochthon developed more distant from magmatism, about 30-40 km SE of the Kane Springs Wash caldera. The detachment is,a normal fault that has exhumed structural depths in its footwall that are in excess of 5000 m (Axen et al., 1990; Swanson et al., 2012).

CARBONATE CLUMPED ISOTOPE THERMOMETRY

Methods

Clumped isotope thermometry is a relatively new technique for measuring the temperature of carbonate mineral crystallization. The bonding of the heavy isotopes ^{13}C and ^{18}O to each other is a temperature-dependent process, and is measurable with current mass spectrometry techniques (Eiler, 2007). This effect can be described as an exchange reaction with the form:

$$Ca^{13}C^{16}O_3 + Ca^{12}C^{18}O^{16}O_2 = Ca^{13}C^{18}O^{16}O_2 + Ca^{12}C^{16}O_3$$

The forward reaction causes “clumping” of the heavy isotopes. The extent to which this forward reaction is favored depends on the balance between the lower vibrational energy of the ^{13}C-^{18}O bond and the entropy of the system, as described in Schauble and others (2006). At higher temperatures, a more random distribution is favored, whereas at lower temperatures, clumping is preferred. This degree of ordering is set during crystallization at temperatures less than ~200 to 300 °C, and readily modified by intracrystalline diffusion at higher temperatures (Eiler, 2007). The measured mass 47, which consists principally of $^{13}C^{18}O^{16}O$, but also minor quantities of $^{12}C^{18}O^{17}O$ and $^{13}C^{17}O_2$, is compared to that expected for a stochastic distribution, and the difference is denoted as Δ_{47}, in units of permil (Eiler, 2011). The raw Δ_{47} values are standardized by comparison to CO_2 gases heated to achieve a nearly stochastic distribution, and then corrected for temperature-dependent fractionation during acid digestion.

Powders were most often obtained by microdrilling, using a 0.5 mm drill bit, to extract 8-12 mg of carbonate from either saw-cut or split samples. Accordingly, features smaller than 5 mm are too small to sample separately using this technique. A few samples (labeled with a C in the sample name, tables 1 and 2) were analyzed as small chips, also weighing 8-12 mg, while a few others (labeled with an M in the sample name, tables 1 and 2) were ground to a powder using a mortar and pestle. Using the sample preparation and analysis techniques described in Huntington and others (2009), the samples were reacted with phosphoric acid at 90 °C to produce CO_2 gas, which was then cleaned by established cryogenic and gas chromatographic methods and measured for masses 44–49 using a Finnegan 253 gas source mass spectrometer.

Measured values for Δ47 for each sample were corrected based on the week's heated gas measurements, and then converted into the absolute reference frame via a secondary transfer function. This function included 25°C water-equilibrated gases, 1000°C heated gases, and carbonate standards with known values in the absolute reference frame (Burgmann, 2013). Then the digestion fractionation value for 90°C acid bath of +0.092‰ was applied. The corrected Δ_{47} values are empirically related to temperature using experimental data from natural and synthetic calcites, aragonites and dolomites (Bonifacie and others, in preparation; Bonifacie and others, 2011).

All stated carbon isotopic ratios are $\delta^{13}C$ with respect to Vienna Pee Dee Belemnite (VPDB), and oxygen isotopic ratios are $\delta^{18}O$ with respect to Vienna Standard Mean Ocean Water (VSMOW). Fractionation factors used to calculate the $\delta^{18}O$ composition of pore waters are from O'Neil and others (1969) and Vasconcelos (2005). Acid digestion fractionation factors were taken from Guo and others (2009) and Rosenbaum and Sheppard (1986). For mixed calcite-dolomite samples, all calculations were done for both end members of pure calcite and pure dolomite, and the $\delta^{18}O$ carbonate and $\delta^{18}O$ water values reflect a weighted average based on estimates of the calcite/dolomite ratios.

Errors are 1-sigma standard errors of the mean, based on the cumulative results of 8 acquisitions of 7 cycles per acquisition, range from 0.0004‰ to 0.011‰ (averaging 0.003‰) in the carbon and oxygen isotope measurements, and from 0.004‰ to 0.021‰ (averaging 0.012‰), for Δ47. These errors in Δ47 propagate into errors in temperature of ±2 to 112°C, depending on the temperature.

We took broad approach to sampling, and analyzed a large number of different textures from different locations, with replications focused on a few key samples. We did this to maximize the odds of finding elevated temperatures from frictional heating, at the expense of more precise temperature values that come from replication. The errors on unreplicated samples presented here are sufficiently small to easily distinguish comminuted host rock material from carbonate that mineralized at temperatures 100-200° higher than the host rock.

Sample Descriptions

A variety of different textures of carbonate were collected from the Mormon Mountains and Heart Mountain areas, and are described in detail below. The Mormon Mountains sampling was focused on the detachment zone, and all samples except the host rock were collected within a meter of main slip surface. Sampling within the Heart Mountain area included both the detachment zone, and samples from hanging wall structures well above the fault. We distinguish the samples here using abbreviations keyed to their locations relative to the detachment surface, with "FW" referring to the footwall, "DET" referring to the detachment plane and samples within c. 10 cm of it, and "HW" referring to the hanging wall, and "host" referring to samples unaffected by faulting.

Host rocks and footwall samples (host and FW): These samples were collected from areas away from fault deformation, to establish a baseline for fault-related effects. In the Mormon Mountains, we use host rock and clast data from Swanson et al. (2012). Host rocks there were collected in Cambrian strata 250-300 meters below the detachment. In Wyoming, Ordovician Bighorn Formation samples were collected from the Rattlesnake anticline (see Figure 6), at least 1 km below any potential eroded detachment surface, and 5 km east of the SE-most exposures. In addition, samples were collected from the Mississippian Madison Formation 10 m above the detachment, from a site near the NW-most exposure of the detachment, and from near the center of detachment exposures, in Cambrian Grove Creek Formation at least 15 meters below the detachment.

Footwall veins (FW-v): are samples of calcite spar that has precipitated in cracks that form within a meter of the detachment. Only veins of at least 2 mm width could supply enough material to analyze, limiting the number of these analyses.

Detachment breccia (DET-b): These samples were all collected from within 1 meter of the detachment surfaces, and predominantly within 10 cm. They consist of a fine-grained matrix and angular clasts, some of which appear to be clasts of an earlier brecciation episode (Figure 1, a, c and d).

Clastic dikes (HW-c): These samples are texturally and lithologically similar to detachment breccias, but are found in irregular dike-like structures at high angles to the detachment. These were only collected from the Heart Mountain allochthon, where their identification was greatly facilitated by the contrast in color with the dark volcanic host rock (see Figure 2 d and e)

Hanging wall veins, void fills, and caliche (HW-v): These hanging wall veins and void fills are sparry calcite and local dolomite. Veins fill parallel-sided fractures that are between 2 mm and 2 cm wide, while void fills have irregular boundaries and may be up to decimeter scale. Two of the veins at Heart Mountain show growth fibers in the calcite. This category also includes vein material that is fine-grained, and texturally similar to calcrete (Figure 2a).

Hanging wall fault breccia (HW-f): These cataclastic rocks were sampled from faults contained entirely within the hanging wall. These were only sampled from Heart Mountain allochthon. Samples are mixtures of the material that comprises the matrix and small clasts of this texture (Figure 2 e and f).

Marble breccia (DET-m): these samples are exclusively from the unique basal cataclasite at White Mountain (Heart Mountain allochthon), where the hanging wall host is metamorphosed by local intrusions. These breccias were sampled from within 3 meters of the detachment, but their unique appearance and proximity to volcanic processes leads us to consider them separately from other detachment breccias (Figure 2c).

Gouge (DET-g for Mormon Mountains, HW-g for Heart Mountain allochthon): These samples are very fine-grained cataclasites with no clasts visible, even with an optical microscope. The Mormon Mountains gouge samples were collected from the detachment surface, while the Heart Mountain gouge samples cam from hanging wall faults, due to lack of carbonate-rich gouges along the detachment.

Mormon Mountains

Geologic background

The Mormon Peak detachment is an extensively exposed low-angle slip surface, active during middle Miocene extension in the Basin and Range province (Wernicke and others, 1985; Axen and others, 1990; Figure 3a). The footwall is a gently east-tilted crustal section through the frontal decollement zone of the Sevier fold-and-thrust belt, with approximately 7 km of pre-tilt structural relief (Figure 3, b and c). The footwall of the detachment is unmetamorphosed and relatively intact structurally, and includes a thrust plate of Cambrian strata structurally overlying sub-thrust Cambrian through Mississippian strata resting nonconformably on early Proterozoic basement. Cambrian through Middle Devonian strata are predominantly dolostone, whereas Upper Devonian and younger strata are primarily limestone, each with relatively minor amounts of chert and siliciclastic strata. In eastern areas of exposure, the detachment cuts across Middle and Upper Cambrian strata of the thrust allochthon. The detachment truncates the thrust, such that in western areas of exposure, the footwall includes only sub-thrust rocks (Figure 3).

The hanging wall of the detachment (Figure 3c) contains Cambrian through Permian carbonates derived from the thrust allochthon, locally overlain by late Oligocene to middle Miocene (*ca*. 23-14 Ma) volcanic and sedimentary strata, all displaced westward relative to footwall rocks (Wernicke and others, 1985; Anderson and others, 2010). Where present, Tertiary strata are approximately concordant with the underlying Paleozoic rocks. The structural depth of the base of hanging wall blocks prior to faulting and tilting was, therefore, not significantly greater than the total stratigraphic thickness of Tertiary and Paleozoic units, which is about 2000 m (Figure 3b).

Exposures of the detachment span an east-west distance of more than 20 km, corresponding to footwall paleodepths of ~2 to 7 km. We collected samples from 6 locations relatively evenly spaced across this transect (Figure 3a), generally within 1 m of the detachment plane.

Isotopic data

A summary of the 54 isotopic analyses for samples from the Mormon Mountain can be found in Table 1, and plotted in Figure 4, color-coded by texture. Forty-two of these analyses are from Swanson et al. (2012) (Chapter 2), and have been sorted into the new texture categories defined here, and included on the plot, with a smaller symbol size to discriminate it from the new data presented here.

Host rock samples (host) have $\delta^{18}O$ values of 22 to 26 permil, $\delta^{13}C$ values of -2 to 2 permil, precipitation temperatures of 80 to 130 °C, and calculated fluid $\delta^{18}O$ values of 3 to 6 permil. These values are those expected to result from the evaporative conditions on a cratonic platform generally associated with dolomitization.

Footwall veins (FW-v) have $\delta^{18}O$ values of 16 to 22 permil, $\delta^{13}C$ values of -3 to 0 permil, precipitation temperatures of 140 to 165 °C, and calculated fluid $\delta^{18}O$ values of 3 to 7 permil. These elevated temperatures suggest formation at depths of ~5 km, assuming a geothermal gradient of approximately 25 °C/km.

Detachment breccias (DET-b) have $\delta^{18}O$ values of 13 to 25 permil, $\delta^{13}C$ values of -6 to 3 permil, precipitation temperatures of 25 to 175 °C, and calculated fluid $\delta^{18}O$ values of -9 to 8 permil. These large ranges likely reflect variation in the proportion of diverse materials contained within the breccias.

Hanging wall veins, void fills, and caliche (HW-v) contain carbonate with $\delta^{18}O$ values of 8 to 21 permil, $\delta^{13}C$ values of -8 to 1 permil, precipitation temperatures of 10 to 115 °C, and calculated fluid $\delta^{18}O$ values of -12 to -5 permil. These highly depleted values of $\delta^{18}O$-water are indicative of a meteoric water source for these materials, with the temperature variations likely reflecting differences in depth at the time of formation, with older samples being warmer and younger samples being colder.

Gouge samples (DET-g) have $\delta^{18}O$ values of 12 to 22 permil, $\delta^{13}C$ values of -8 to 2 permil, precipitation temperatures of 5 to 250°C, and calculated fluid $\delta^{18}O$ values of -12 to 11 permil. These large ranges are similar to those of the breccias, and probably also reflect the variable proportions of diverse materials contained within these mixtures. The two warmest DET-g temperatures are, however, 60-80 °C warmer than the warmest DET-b temperatures.

Discussion

The samples that appear to be mixtures (i.e. DET-b and DET-g) show carbon and oxygen isotopic compositions that could result from combining fragments of the host rock, warm vein material, and cold vein material. But the higher temperatures require an additional source that crystallized under hot conditions.

The highest temperatures measured in the Mormon Mountains, 240-250°C, are found within a thin (c. 1 cm) layer of gouge collected from the main slip surface near Mormon Peak (ES10-23, Figure 5). This sample shows 3 layers parallel to the detachment slip surface that are distinct in color in hand sample. Each layer has similar oxygen and carbon isotopic compositions ($\delta^{18}O$ values of 19.1-20.1 permil, $\delta^{13}C$ values of -1.1 to -1.8 permil), but strongly contrasting temperatures, with the bottom layer averaging 40°C, the middle layer averaging 110°C, and the top layer averaging 245°C. X-ray diffraction analyses indicate this top layer is nearly pure dolomite, with no trace of Ca or Mg oxides or hydrated oxides, and SEM imagery shows an extremely fine grain size, not well distinguished even with the SEM. The middle layer is compositionally and isotopically identical to the host rock, but calcite microveins cross-cut the layer, which also contains local euhedral iron oxides. The lower, colder layer shows a larger variety of textures and materials, with the predominant carbonate mineral being calcite. This mineral is present in cross-cutting veins, as well as in the breccia matrix. The cold layer contains a clast of the middle layer within it, but there are no clear cross-cutting relationships between the middle layer and the warmest top layer.

This 200°C temperature difference thus occurs over less than 1 cm, and in a sample directly on the detachment surface. The 250°C temperature is hotter than ambient conditions the fault rock would have experienced, with the footwall at that location predicted to have been no deeper than ~4-5 km. With a surface temperature of 25°C and a geothermal gradient of 25°C/km, temperatures would be expected to be 150°C or colder.

There is a subtle effect of grain size on the recorded temperatures. The fine-grained gouges (DET-g) show a larger variation in temperatures than the coarser breccias (DET-b), with the gouges recording more extreme temperatures at both the cold and hot ends of the spectrum. The hotter end might contain a higher proportion of frictionally heated material. If the gouges and breccias just represent mixtures of pre-existing material, it is difficult to explain the gouges with temperatures of less than 20°C, while breccias record temperatures down to 25 °C. Presumably it would take more time on a fault to be comminuted to gouge, and therefore older, deeper material should be incorporated. Instead the 5-15 degree temperatures are found in the finest textures. This may represent the effect of late meteoric fluids on the fault, with the alteration affecting small grain sizes more strongly.

Heart Mountain

Geologic Background

The Heart Mountain detachment is a low-angle slip surface that is currently exposed in a ~70 km by 30 km area, with apparent slip of as much as 45 kilometers (Pierce, 1980, Figure 6). At present, the base of the allochthon is subhorizontal (<10° dip), and exposures of the upper plate of the detachment, the Heart Mountain allochthon, form internally coherent masses that show evidence of mild internal extension.

The allochthon contains two main components, a thin, cratonic Paleozoic section ranging from Ordovician to Mississippian in age, overlain by Eocene (c. 52-48 Ma) volcanic strata of the Absaroka Volcanic Supergroup and related dikes and small intrusive bodies. The fault initially localized within a narrow stratigraphic interval (<5 m) near the base of the Ordovician Bighorn Formation, but because of internal distension of the allochthon, both its Paleozoic and Tertiary components lie along the fault plane (e.g. Hauge , 1985, 1990). The fault lies along the eastern margin of the extensive Absaroka volcanic field, and was active during Absaroka magmatism (e.g. Hiza, 2000; Feeley and Cosca, 2003; Douglas et al., 2003).

Isotopic data

A summary of the isotopic data for the 83 samples from Heart Mountain can be found in Table 2, and plotted keyed by texture in Figure 7.

Host rock samples (host) have $\delta^{18}O$ values of 22 to 27 permil and $\delta^{13}C$ values of -2 to 4 permil. Precipitation temperatures are 50 to 65°C for the Paleozoic units, and 40°C for a single sample of the Jurassic Sundance Formation. Calculated fluid $\delta^{18}O$ values are -4 to 4 permil, and likely reflect formation and burial diagenesis conditions.

The sole footwall vein (FW-v) collected that was large enough to analyze has a $\delta^{18}O$ value of 22.4 permil, a $\delta^{13}C$ value of 0 permil, precipitation temperatures of 56°C, and calculated fluid $\delta^{18}O$ value of -3.3 permil. These values are within the range of Cambrian host values.

Detachment breccias (DET-b) have $\delta^{18}O$ values of 12 to 30 permil, $\delta^{13}C$ values of -3 to 4 permil, precipitation temperatures of 14 to 90 °C, and calculated fluid $\delta^{18}O$ values of -12 to 8 permil. These large ranges reflect the variation of materials contained within these mixtures.

Marble breccia (DET-m) samples have $\delta^{18}O$ values of 21 to 27 permil, $\delta^{13}C$ values of -3 to -2 permil, precipitation temperatures of 145 to 335°C, and calculated fluid $\delta^{18}O$ values of 13 to 18 permil. These ranges are narrow relative to other textures, and likely formed during metamorphic reactions immediately following the intrusion of hot volcanic material. The white color and marble texture of the host in this location supports this interpretation, and is not found near any of the other samples.

Clastic dikes (HW-c) contain carbonate with $\delta^{18}O$ values of 10 to 25 permil, $\delta^{13}C$ values of -2 to 1 permil, precipitation temperatures of 35 to 75 °C, and calculated fluid $\delta^{18}O$ values of -12 to 4 permil. These large ranges reflect the variety of carbonate sources contained within these mixtures.

Hanging wall veins and void fills (HW-v) have $\delta^{18}O$ values of 11 to 22 permil, $\delta^{13}C$ values of -4 to 3 permil, precipitation temperatures of 25 to 65°C, and calculated fluid $\delta^{18}O$ values of -13 to -6 permil. These values of $\delta^{18}O$-water are indicative of a meteoric water source for these materials, with the temperature variations likely reflecting differences in depth at time of formation.

Hanging wall fault breccias (HW-f) have $\delta^{18}O$ values of 17 to 26 permil, $\delta^{13}C$ values of -3 to 0 permil, precipitation temperatures of 75 to 335°C, and calculated fluid $\delta^{18}O$ values of 0 to 19 permil. These values, particularly the high temperatures, are unlike any of the source materials.

Gouge samples (HW-g) have $\delta^{18}O$ values of 18 to 31 permil, $\delta^{13}C$ values of -3 to 4 permil, precipitation temperatures of 30 to 215 °C, and calculated fluid

$\delta^{18}O$ values of -11 to 14 permil. These large ranges reflect the variation of materials contained within these mixtures.

The samples that are mixtures (DET-b, HW-c, HW-f, and HW-g) shows carbon and oxygen isotopic compositions of carbonate that could result from mixtures of the host rock, warm vein material, and cold vein material, but the higher temperatures of HW-f, and HW-g require an additional source material that crystallized under hot conditions.

Discussion

While a few samples from the hanging wall yielded high temperatures, the majority of the samples are cold. Of the 83 samples, 63 had average crystallization temperatures under 100°C, a highly counterintuitive finding given that the Heart Mountain detachment essentially accommodates the collapse of an active volcanic center. Where is the evidence of hydrothermal fluids? Also enigmatic is the location of the hot samples: while the 6 samples from White Mountain all record temperatures of at least 140°C, the remaining 14 samples with temperatures over 100°C come from hanging wall faults in areas with no volcanic rocks in the immediate vicinity, and which now lie away from volcanic centers on the periphery of the allochthon.

Possible sources of heat for these samples are: direct contact with volcanic or plutonic rocks (i.e., contact metamorphism), elevated geothermal gradient due to the 1-3 km thick stack of volcanics above, and frictional heating along the faults during slip.

The first possibility is not favored due to the lack of proximal exposures of volcanic rocks, and the sedimentary, not metamorphic, textures of these rocks. The second possibility is more plausible, but there is, if anything, an *anti*correlation between samples recording the hottest temperatures and proximity to the volcanic centers, with no volcanics surviving erosion above them. In contrast, samples from areas that lie beneath kilometer-scale thicknesses of volcanic rocks show temperatures that are barely elevated, on the order of ~10°C above the host rock temperature. Given this disparity, we prefer the scenario where the heat recorded within the hanging wall faults owes its origin to frictional heating during slip.

The oxygen isotopic composition of water calculated to be in equilibrium with the high-temperature carbonate samples is enriched in $\delta^{18}O$ relative to all the source materials. Assuming these carbonates precipitated while in equilibrium with the surrounding fluid, this fluid must have had a very low water-to-rock ratio, given $\delta^{18}O$ values of up to 19 permil. Waters this enriched are not commonly described, and may not reflect the composition of a large body of water. They likely result either from a closed, rock-buffered system, or may reflect the reordering of dolomite at temperatures above 250°C without the effect of fluids.

Of all the detachment breccia (DET-b) and clastic dike (HW-c) samples we analyzed (n=37), *not one is hotter than 90°C*. There are two main possibilities for this observation: either no heat was present during crystallization, or it was present, but not preserved. Preservation of a heating signal would not occur if carbonate minerals did not recrystallize under hot conditions, if the hot material later recrystallized under cold conditions, the hot material was later removed via tectonics or dissolution, or the hot carbonate was overwhelmed by volumetrically more significant cold material.

Given that hanging wall faults can preserve this heating signal, we prefer the interpretation that the hot carbonate existed while the detachment was at depth, but got overprinted by further fluid infiltration/slip events. It is plausible that displacement on the detachment occurred by aseismic creep and was therefore not heated frictionally, while seismic slip occurred on the hanging wall faults. But given the similar isotopic compositions between the two, we think it more likely that the main fault was more thoroughly overprinted by late-stage fluid infiltration than hanging wall faults. This could arise from the more protracted slip history on the main detachment than on any given hanging wall splay.

The hanging wall faults we sampled are both at low angles to the main detachment, (dipping <30°), and they both have a similar burrowed texture of Bighorn Formation in their footwalls, and brecciated Bighorn Formation in their hanging walls. They are lie towards the “toe” or “runout” area of the Heart Mountain allochthon, with the Steamboat site at the bottom of the “transgressive zone”, a region that cuts up-section and up-hill eastwards towards the Bighorn Basin, and Heart Mountain within the Bighorn Basin. Given these locations, the allochthon might be expected to have experienced a degree of horizontal contraction, and as such we suspect that these low-angle faults might actually be pieces of detachment that were excised from the footwall, resulting in fragments of the detachment and footwall interposed between hanging wall blocks.

In the case of the Heart Mountain samples, it is clear that this fault experienced many episodes of slip, with gouge overprinting breccia, only to be incorporated as clasts in a later breccia. Additionally, a void fill sample that overprints the breccia gives two temperatures of 55 and 60°C, which precludes its formation as a late-stage, near surface in-fill. It may have formed immediately post-slip, during cooling of the slip event, or it may have formed in the fault zone at 1-2 km depth, depending on the local geothermal gradient.

Comparison of the Mormon Peak and Heart Mountain Allochthons

The distributions of stable and clumped isotopic compositions show broadly similar trends for both the Mormon Mountains and Heart Mountains (Figures 8). The majority of samples have compositions that can be explained by mixtures of host rock, veins, and a higher-temperature material. A summary of the different characteristics of each of these materials can be found in Table 3, and a schematic representation of the large-scale similarities and differences between the two detachment systems is depicted in Figure 9. In fine-grained breccias or gouges, it can be difficult to distinguish these materials without the temperature information from clumped-isotope thermometry.

The highest temperatures reach at least 250°C for both areas, and show textural evidence of frictional heating. Both areas of study show isotopic evidence for the predominant source of water along the fault being meteoric. Despite proximity to volcanic centers, there is little evidence in either area for precipitation of carbonate from any magma-derived fluids.

A major difference between the two study areas is the paleodepths sampled by the fault rocks (Figure 9). The Mormon Peak detachment has rocks in its footwall that were at depths of as much as c. 6 km during slip. In contrast, the Heart Mountain allochthon, being rootless, never reached depths of greater than 2 kilometers. This difference is reflected in the temperatures of the warmest veins, with the warmest vein at Heart Mountain recording a temperature of 65°C, much colder than the 165°C vein temperatures from the footwall of the Mormon Peak allochthon.

An interesting finding is that samples from the Mormon Mountains are generally warmer than their textural equivalents in the Heart Mountain area. This would not be expected if magmatic processes were intimately related to slip processes along the fault, because the Mormon Mountains are significantly further from magmatic centers. Instead, the ambient temperatures owing to paleodepth seem to play a dominant role.

Sample temperatures that do not appear to be controlled by ambient conditions include the hottest samples, which we interpret to be frictionally heated. These were more frequently sampled from the Heart Mountain area, but are found in the Mormon Mountains as well directly on the detachment surface. The preservation of the heating signal appears to be better in hanging wall faults, which were not sampled in the Mormon Mountain, but both areas have samples over 200°C. There is a possibility the hot samples from the Mormon Mountains were originally on a hanging wall fault that was faulted down onto the detachment surface, but it is also possible these samples were heated while on the detachment.

The better preservation of hot samples along hanging wall faults might be the result of “isolation” from fluid flow along the detachment during later events, while motion on hanging wall faults may a much more limited history of slip and fluid flow. It seems likely that with continued slip and permeability enhancement, authigenic carbonate precipitated from meteoric water comprises an increasing proportion of the carbonate in fault zone rocks.

Conclusions

Carbonate clumped-isotope ratios are capable of recording the transient elevation of temperatures from frictional heating along detachments, although preservation along the main detachment surfaces is not common. It is possible that hanging wall faults related to slip on these surfaces, or fragments of the detachment incorporated into the allochthons, better preserved the record of frictional heating.

Magmatic processes appear to play a very minor role, if any, in the carbonate isotopic signature along either the Mormon Mountain of Heart Mountain detachments. The majority of fault zone material is depleted in $\delta^{18}O$ and cold relative to the host rock, indicating the addition of material that precipitated from meteoric water.

References

Aharonov, E., and Anders, M. H., 2006, Hot water: A solution to the Heart Mountain detachment problem?: Geology, v. 34, no. 3, p. 165.

Anders, M. H., Christie-Blick, N., and Walker, C. D., 2006, Distinguishing between rooted and rootless detachments: A case study from the Mormon Mountains of southeastern Nevada: Journal of Geology, v. 114, no. 6, p. 645-664.

Anders, M. H., Fouke, B. W., Zerkle, A. L., Tavarnelli, E., Alvarez, W., and Harlow, G. E., 2010, The Role of Calcining and Basal Fluidization in the Long Runout of Carbonate Slides: An Example from the Heart Mountain Slide Block, Wyoming and Montana, U.S.A: The Journal of Geology, v. 118, no. 6, p. 577-599.

Anderson, R. E., Felger, T.J., Diehl, S.F., Page, W.R., Workman, J.B., 2010, Integration of tectonic, sedimentary and geohydrologica processes leading to small-scale extension model for the Mormon mountains area north of Lake Mead, Lincoln County, Nevada, *in* Umhoefer, P. J., Beard, L.S., Lamb, M.A. (Eds.), ed., Miocene Tectonics of the Lake Mead Region, Central Basin and Range, Geological Society of America Special Paper 463, p. pp. 395-426.

Axen, G. J., 2004, Mechanics of low-angle normal faults, *in* Karner, G. D., Taylor, B., Driscoll, N. W., and Kohlstedt, D. L., eds., Rheology and deformation of the lithosphere at continental margins: New York, Columbia University Press, p. 46–91.

Axen, G. J., Wernicke, B. P., Skelly, M. F., and Taylor, W. J., 1990, Mesozoic and Cenozoic tectonics of the Sevier thrust belt in the Virgin River valley area, southern Nevada Basin and Range extensional tectonics near the latitude of Las Vegas, Nevada: Geological Society of America Memoir, v. 176, p. 123-153.

Beutner, E. C., and Hauge, T. A., 2009, Heart Mountain and South Fork fault systems: Architecture and evolution of the collapse of an Eocene volcanic system, northwest Wyoming: Rocky Mountain Geology, v. 44, no. 2, p. 147–164.

Cowan, D. S., 1999, Do faults preserve a record of seismic slip? A field geologist's opinion: Journal of Structural Geology, v. 21, p. 995–1001.

De Paola, N., Chiodini, G., Hirose, T., Cardellini, C., Caliro, S., and Shimamoto, T., 2011, The geochemical signature caused by earthquake propagation in carbonate-hosted faults: Earth and Planetary Science Letters, v. 310, no. 3-4, p. 225-232.

Diehl, S. F., Anderson, R.E., and Humprey, J.D., , 2010, Fluid flow, solution collapse, and massive dissolution at detachment faults, Mormon Mountains, Nevada, *in* Umhoefer, P. J., Beard, L.S., and Lamb, M.A. (Eds.), ed., Miocene Tectonics of the Lake Mead Region, Central Basin and Range, Geological Society of America Special Paper 463, p. 427-441.

Douglas, T. A., Chamberlain, C. P., Poage, M. A., Abruzzese, M., Schultz, S., Henneberry, J., and Layer, P., 2003, Fluid flow and the Heart Mountain fault: a stable isotopic, fluid inclusion, and geochronologic study: Geofluids, v. 3, p. 13-32.

Eiler, J. M., 2007, "Clumped-isotope" geochemistry—The study of naturally-occurring, multiply-substituted isotopologues: Earth and Planetary Science Letters, v. 262, p. 309–327.

Eiler, J. M., 2011, Paleoclimate reconstruction using carbonate clumped isotope thermometry: Quaternary Science Reviews, v. 30, no. 25-26, p. 3575–3588.

Feeley, T. C., and Cosca, M. A., 2003, Time vs. composition trends of magmatism at Sunlight volcano, Absaroka volcanic province, Wyoming: Geological Society of America Bulletin, v. 115, no. 6, p. 714–728.

Guo, W. F., Mosenfelder, J. L., Goddard, W. A., III, and Eiler, J. M., 2009, Isotopic fractionations associated with phosphoric acid digestion of carbonate minerals: Insights from first-principles theoretical modeling and clumped isotope measurements: Geochimica et Cosmochimica Acta, v. 73, no. 24, p. 7203–7225.

Han, R., Hirose, T., and Shimamoto, T., 2010, Strong velocity weakening and powder lubrication of simulated carbonate faults at seismic slip rates: Journal of Geophysical Research, v. 115, no. B3.

Hauge, T. A., 1985, Gravity-Spreading origin of the Heart Mountain allochthon, northwestern Wyoming: Geological Society of America Bulletin, v. 96, p. 1440-1456.

Hauge, T. A., 1990, Kinematic model of a continuous Heart Mountain allochthon: Geological Society of America, v. 102, p. 1174-1188.

Hickman, S., and Zoback, M., 2004, Stress orientations and magnitudes in the SAFOD pilot hole: Geophysical Research Letters, v. 31, no. 15.

Hirose, T., and Shimamoto, T., 2005, Growth of a molten zone as a me- chanism of slip weakening of simulated faults in gabbro during frictional melting: Journal of Geophysical Research, v. 110, no. B05202.

Hiza, M. M., 2000, The Geochemistry and Geochronology of the Eocene Absaroka Volcanic Province, Northern Wyoming and Southwest Montana, USA [Doctor of Philosophy: Oregon State University, 240 p.

Hughes, C. J., 1970, The Heart Mountain detachment fault: a volcanic phenomenon?: Journal of Geology, v. 78, no. 107-116.

Huntington, K. W., Eiler, J. M., Affek, H. P., Guo, W., Bonifacie, M., Yeung, L. Y., Thiagarajan, N., Passey, B., Tripati, A., Daeron, M., and Came, R., 2009, Methods and limitations of "clumped" CO2 isotope (Δ_{47}) analysis by gas-source isotope ratio mass spectrometry: Journal of Mass Spectrometry, v. 44, no. 9, p. 1318 –1329.

Lister, G. S., and Baldwin, S. L., 1993, Plutonism and the origin of metamorphic core complexes: Geology, v. 21, p. 607-610.

Lister, G. S., and Davis, G. A., 1989, The origin of metamorphic core complexes and detachment faults formed during Tertiary continental extension in the northern Colorado River region, U.S.A: Journal of Structural Geology, v. 11, p. 65–94.

Livaccari, R. F., and Geissman, J. W., 2001, Large-magnitude extension along metamorphic core complexes of western Arizona and southeastern

California: Evaluation with paleomagnetism: Tectonics, v. 20, no. 5, p. 625-648.

Lockner, D. A., Morrow, C., Moore, D., and Hickman, S., 2011, Low strength of deep San Andreas fault gouge from SAFOD core: Nature, v. 472, no. 7341, p. 82-85.

Losh, S., 1997, Stable isotope and modeling studies of fluid-rock interaction associated with the Snake Range and Mormon Peak detachment faults, Nevada: Geological Society of America Bulletin, v. 109, no. 3, p. 300 –323.

Melosh, H. J., 1990, Mechanical basis for low-angle normal faulting in the Basin and Range province: Nature, v. 343, p. 331–335.

Morley, C. K., 2014, The widespread occurrence of low-angle normal faults in a rift setting: Review of examples from Thailand, and implications for their origin and evolution: Earth-Science Reviews, v. 133, no. 0, p. 18-42.

Mount, V. S., and Suppe, J., 1987, State of stress near the San Andreas fault: Implications for wrench tectonics: Geology, v. 15, no. 12, p. 1143-1146.

O'Neil, J. R., Clayton, R. N., and Mayeda, T. K., 1969, Oxygen isotope fractionation in divalent metal carbonates: Journal of Chemical Physics, v. 51, p. 5547–5558.

Parsons, T., and Thompson, G. A., 1993, Does magmatism influence low-angle normal faulting?: Geology, v. 21, no. 3, p. 247-250.

Pierce, W. G., 1980, The Heart Mountain break-away fault, northwestern Wyoming: Geological Society of America Bulletin, v. 91, p. 272-281.

Rice, J. R., 1992, Chapter 20 Fault Stress States, Pore Pressure Distributions, and the Weakness of the San Andreas Fault, *in* Brian, E., and Teng-fong, W., eds., International Geophysics, Volume Volume 51, Academic Press, p. 475-503.

Rice, J. R., 2006, Heating and weakening of faults during earthquake slip: Journal of Geophysical Research, v. 111.

Rosenbaum, J., and Sheppard, S. M. F., 1986, An isotopic study of siderites, dolomites and ankerites at high temperatures: Geochimica et Cosmochimica Acta, v. 50, no. 6, p. 1147–1150.

Schauble, E. A., Ghosh, P., and Eiler, J. M., 2006, Preferential formation of ^{13}C-^{18}O bonds in carbonate minerals, estimated using first-principles lattice dynamics: Geochimica et Cosmochimica Acta, v. 70, no. 10, p. 2510 –2529.

Scott, R. B., Unruh, D. M., Snee, L. W., Harding, A. E., Nealey, L. D., Blank, H. R., Budahn, J. R., and Mehnert, H. H., 1995, Relation of peralkaline magmatism to heterogeneous extension during the middle Miocene, southeastern Nevada: Journal of Geophysical Research: Solid Earth (1978–2012), v. 100, no. B6, p. 10381-10401.

Scott, R. J., and Lister, G. S., 1992, Detachment faults:Evidence for a low-angle origin: Geology, v. 20, no. 9, p. 833-836.

Sibson, R. H., 1975, Generation of pseudotachylyte by ancient seismic faulting: Geophys J. R. Astron. Soc, v. 43, p. 775–794.

Smedes, H. W., and Prostka, H. J., 1972, Stratigraphic framework of the Absaroka Volcanic Supergroup in the Yellowstone National Park region: U.S. Geological Survey Professional Paper, v. 729-C, p. 1–33.

Sulem, J., and Famin, V., 2009, Thermal decomposition of carbonates in fault zones: Slip-weakening and temperature-limiting effects: Journal of Geophysical Research, v. 114, no. B3.

Swanson, E. M., Wernicke, B. P., Eiler, J. M., and Losh, S., 2012, Temperatures and Fluids on Faults Based on Carbonate Clumped-Isotope Thermometry: American Journal of Science, v. 312, no. 1, p. 1-21.

Templeton, A. S., Sweeney, J. J., Manske, H., Tilghman, J. F., Calhoun , S. C., Violich, A., and Chamberlain, C. P., 1995, Fluids and the Heart Mountain fault revisited: Geology, v. 23, no. 10, p. 929-932.

Vasconcelos, C., McKenzie, J. A., Warthmann, R., and Bernasconi, S. M., 2005, Calibration of the $\delta^{18}O$ paleothermometer for dolomite precipitated in microbial cultures and natural environments: Geology, v. 33, no. 4, p. 317–320.

Walker, C. D., Anders, M. H., and Christie-Blick, N., 2007, Kinematic evidence for downdip movement on the Mormon Peak detachment: Geology, v. 35, no. 3, p. 259.

Wernicke, B., 1995, Low-angle normal faults and seismicity: A review: Journal of Geophysical Research, v. 100, no. B10, p. 20159.

Wernicke, B., Walker, J. D., and Beaufait, M. S., 1985, Structural Discordance between Neogene Detachments and Frontal Sevier Thrusts, Central Mormon Mountains, Southern Nevada: Tectonics, v. 4, no. 2, p. 213-246.

Yin, A., 1989, Origin of Regional, Rooted Low-Angle Normal Faults - A Mechanical Model and its Tectonic Implications: Tectonics, v. 8, no. 3, p. 469-482.

Tables

Table 1. Summary of samples from the Mormon Mountains, NV[a]

sample	site	$\delta^{13}C$	$\delta^{18}O$	T	$\delta^{18}O_w$
HW-v					
ES10-21 T4	2	-5.07	20.2	11.8	-10.78
ES10-32 T2 14	4	-8.02	20.0	36.5	-5.78
ES10-35 T1	4	-7.57	18.6	25.4	-9.39
ES09-04 D1	3	0.78	9.2	84.3	-9.17
ES10-05 D1	1	0.36	10.2	73.0	-9.60
ES10-05 D2	1	0.91	12.1	78.6	-7.04
ES10-22 T2	2	-5.75	19.0	25.7	-8.92
ES10-33 T1	4	-7.80	18.3	28.4	-9.01
FW-v					
ES12-13 T2	6	0.11	21.5	143.2	5.31
ES12-12 T1	6	-0.29	21.4	164.3	6.99
DET-b					
120107-01	5	-1.05	18.8	130.2	1.59
120107-1b	5	0.25	23.9	118.8	5.57
ES12-14	6	1.59	13.5	88.7	-6.11
ES12-14 T4	6	2.13	22.2	93.3	3.00
ES12-16 T1	6	-0.02	21.4	154.3	6.35
ES10-23 D2	2	-1.06	19.1	170.4	4.81
ES10-23 M5P1	2	-1.80	19.3	118.4	1.05
ES10-23 M5P2	2	-1.80	19.3	105.8	-0.20
ES10-23 M7	2	-1.35	20.1	35.0	-7.51
ES10-25 T5	2	-5.21	18.9	37.0	-6.76
ES10-27 T1	2	-4.08	20.3	35.5	-5.70
ES10-27 T2	2	-4.93	19.0	25.2	-9.05
ES12-13	6	-0.13	22.0	142.2	5.99
ES12-03 T2	5	-2.87	20.9	74.0	-0.64
ES12-03 T3	5	-2.53	21.7	111.4	4.40
ES12-06 T1	5	-0.34	17.5	105.1	-1.98
ES12-06 T2	5	-0.65	15.5	160.0	0.56
ES12-06 T3	5	-0.61	15.7	171.8	1.48
ES12-06 T4	5	-0.53	15.7	161.9	1.26
ES12-18	6	-0.04	23.0	110.1	4.24
ES12-18 T1	6	-0.09	22.8	121.0	4.72
ES12-18 T2	6	-0.07	22.7	146.3	7.03
ES12-20	6	-0.12	21.8	174.7	8.02
ES12-19 T4	6	0.45	16.9	110.7	-1.67
ES12-19 T6	6	1.67	19.6	112.4	1.07

ES12-17 T1	6	-0.82	21.0	101.2	1.39
ES12-05 T2	5	-2.57	19.9	86.7	-0.02
ES10-32 T1	4	1.80	24.8	81.8	5.80
DET-g					
ES12-19	6	1.71	17.1	125.8	-0.14
ES12-19 T7	6	1.04	12.3	101.5	-7.17
ES12-01 M1	5	0.90	21.2	95.2	2.24
ES12-10	6	-1.64	21.9	143.3	5.99
ES12-04 T1 S2	5	-5.68	20.7	17.7	-8.95
ES12-04 T1S1	5	-5.64	20.8	6.3	-11.61
ES12-04 T2	5	-5.09	19.4	11.2	-11.71
ES12-05 T1	5	-1.62	20.3	108.3	2.68
ES12-11 T1	6	-0.11	21.9	126.0	4.57
ES10-23 M6P1	2	-1.15	20.8	240.6	10.06
ES10-23 M6P2	2	-1.16	20.8	252.3	10.52
ES12-15 T1	6	2.00	18.0	86.5	-3.20
ES10-25 T3	2	-5.35	19.2	29.2	-8.04
ES10-23 T5	2	-1.45	20.7	143.8	4.83
ES10-35 T2	4	-7.05	19.2	32.7	-7.35
ES12-03 T1	5	-4.35	19.1	50.5	-5.83

[a]Site number locations shown in Figure 3. Carbon isotopes are with respect to VPDB, Oxygen isotopes are with respect to VSMOW, T is temperature in °C; $\delta^{18}O_w$ is the composition of fluid in equilibrium with carbonate, with respect to VSMOW.

Table 2. Summary of isotopic data from the Heart Mountains samples, WY and MT[a]

sample	site	$\delta^{13}C$	$\delta^{18}O$	T	$\delta^{18}O_w$
DET-m					
ES-HM12-06	WM	-2.18	22.63	227.3	14.42
ES-HM12-06	WM	-2.11	22.68	333.2	18.06
ES-HM12-04 T2	WM	-2.35	22.61	231.4	14.59
ES-HM12-06 T5	WM	-2.66	21.47	253.0	14.70
TH-HM12-01	WM	-2.76	26.46	146.0	13.42
ES-HM12-03 T1	WM	-2.22	22.45	312.3	17.27
HW-c					
ES-HM13-01 T2	SF	-1.93	18.52	40.6	-6.51
ES-HM12-13 T1	JS	-1.29	12.11	54.0	-11.46
ES-HM13-41 TD	FC	-0.48	24.59	36.2	-4.20
ES-HM13-41 TE	FC	-0.55	24.78	42.2	-2.95
ES-HM13-41 TF	FC	-0.56	24.92	41.4	-2.94
ES-HM13-41 TA2	FC	-0.48	24.98	55.5	-0.56
ES-HM13-41 TB2	FC	-0.47	24.96	51.4	-1.24
ES-HM13-41 TC2	FC	-0.53	25.01	53.0	-0.93

ES-HM13-39	FC	-0.70	22.33	44.0	-3.76
ES-HM13-29 T1	CR	-0.25	24.50	72.2	3.94
ES-HM13-24 T2	CR	-1.04	21.03	86.6	1.06
ES-HM12-23 T1	CC	-0.94	10.49	73.8	-12.12
ES-HM12-23 T3	CC	0.37	22.21	66.2	-1.70
ES-HM12-19a M1	SG	0.51	12.88	67.0	-9.42
HW-g					
ES-HM12-16 M3	SG	2.42	28.30	62.6	5.99
ES-HM12-32 T2	SB	-0.75	26.78	189.7	13.51
ES-HM12-39 M2	HM	-2.83	19.89	213.2	8.27
ES-HM12-33a T1	SB	-0.57	23.92	98.8	3.63
ES-HM12-40	HM	-2.41	19.50	184.3	6.36
ES-HM12-30 M1	SB	-0.60	24.15	55.3	-1.72
ES-HM13-43 T1	DH	3.22	29.04	39.6	3.57
ES-HM13-42 T1 S1	DH	-0.04	26.42	78.3	6.97
ES-HM13-19H T2	HM	2.27	30.41	46.6	3.29
ES-HM12-40 M1	HM	-1.52	17.79	29.5	-10.86
ES-HM13-44 T1	DH	2.68	30.78	41.8	5.68
ES-HM13-12 T1	SHP	-1.50	25.37	72.3	1.90
ES-HM13-19H T1	HM	3.18	30.41	50.3	3.91
host					
ES-HM12-18 T1	SG	3.68	26.71	60.0	4.68
BW-HM12-10	host	-1.25	22.64	55.9	-3.11
ES-HM12-34T1	HM	-1.78	23.64	64.5	0.74
ES-HM13-02 T1	SF	2.85	22.16	39.5	-3.16
ES-HM12-24 T2	CC	-0.44	22.44	61.9	-2.41
ES-HM12-24 T4	CC	-0.44	22.75	50.1	-3.91
HW-f					
ES-HM12-41 T2	HM	-2.09	19.55	121.1	3.19
ES-HM12-39 M1	HM	-2.71	20.18	154.2	5.11
ES-HM12-35 T3	HM	-1.78	20.42	95.9	1.54
ES-HM12-34 T4	HM	-2.73	17.40	120.9	1.07
ES-HM12-35 T4	HM	-2.67	20.65	133.8	5.36
ES-HM12-34 T3	HM	-2.14	21.10	77.3	0.00
ES-HM12-33a M1	SB	-0.62	26.22	95.2	5.50
ES-HM12-34T2	HM	-1.21	23.50	256.7	15.08
ES-HM12-32 T1	SB	-0.15	25.29	102.3	5.34
ES-HM12-41 T1	HM	-0.86	23.82	106.8	6.02
ES-HM12-35 T1	HM	-2.63	19.88	121.0	3.50
ES-HM12-35 T2	HM	-1.83	21.67	556.5	19.18
ES-HM12-35 T5	HM	-2.56	21.10	269.8	13.18
ES-HM12-35 T6	HM	-1.38	21.44	335.9	14.04
DET-b					

ES-HM13-37 T2	FC	-1.01	22.28	50.2	-4.04
ES-HM13-38	FC	-0.92	20.07	14.2	-10.68
ES-HM13-37 T1	FC	-0.98	22.31	46.3	-4.65
ES-HM13-37 T3	FC	-1.18	22.40	55.9	-3.01
ES-HM13-06 T1	SHP	-0.63	23.91	55.6	-1.92
ES-HM13-28 T1	CR	1.32	21.05	72.4	0.91
ES-HM12-20 T3	CC	-0.43	22.52	54.3	-3.47
ES-HM12-20 T1	CC	0.63	20.27	71.2	-3.24
ES-HM12-14T2	SG	3.95	29.97	62.0	8.18
ES-HM12-31 T3	SB	-1.32	24.92	69.1	1.03
ES-HM12-31 T1	SB	-1.37	25.49	87.5	3.91
ES-HM12-31 T1	SB	-1.35	25.64	74.2	2.41
ES-HM12-15	SG	-1.43	24.39	71.7	0.85
ES-HM12-09 T2	JS	-1.57	17.61	79.7	-3.12
ES-HM12-10 M1	JS	-3.09	11.96	53.3	-11.41
ES-HM12-21 T4	CC	-1.42	22.02	70.7	-1.59
ES-HM12-07 T2	JS	-1.54	15.86	75.4	-5.37
ES-HM12-12 T1	JS	-2.00	22.57	75.0	-0.49
ES-HM12-09 T1	JS	-1.27	22.53	76.5	1.30
ES-HM12-09 T5	JS	-1.28	24.06	61.4	0.70
ES-HM12-09 T3	JS	-2.00	22.37	50.1	-2.70
ES-HM12-09 T4	JS	-1.83	24.00	60.6	0.52
ES-HM12-21 T1	CC	1.39	22.82	77.2	0.04
FW-v					
ES-HM12-27 M1	CC	-0.04	22.40	56.2	-3.30
HW-v					
ES-HM12-05	WM	2.58	22.14	24.2	-6.18
ES-HM12-41 C2	HM	-3.28	15.41	55.2	-7.11
ES-HM12-41 C1	HM	-3.43	15.44	59.8	-6.36
ES-HM13-35 T1	FC	-2.12	15.60	50.0	-7.74
ES-HM13-30 T1	CR	-1.26	11.86	43.7	-12.46
ES-HM13-08 C1	SHP	-1.37	11.80	66.2	-9.01

[a]Site locations as in Figure 5. Carbon isotopes are with respect to VPDB, Oxygen isotopes are with respect to VSMOW, T is temperature in °C; $\delta^{18}O_w$ is the composition of fluid in equilibrium with carbonate, with respect to VSMOW.

Table 3. Summary of the three types of materials found in fault breccias and gouges associated with the Heart Mountain (HM) and the Mormon Peak (MP) detachments.

Material type:	Host rock	Syn-tectonic or immediately post-tectonic conditions	Authigenic fault carbonate
Grain size	10-100 microns	Sub-micron to 10 microns (?)	Sub-micron to mm
mineralogy	Dolomite, local calcite in M/D units	both	Generally calcite, local dolomite
Temperature	55-65° for HM 80-110° for MP	Closure temperatures, 250°C+	Ambient: 100° or less, depending on depth
$\delta^{18}O$-water	~ 0‰	Closed system, so dependent on T	Between -12‰ and ~0‰
$\delta^{13}C$	-2 to +2‰ generally, 4‰ for Madison	Same as host	Same as host, or may be depleted
Ideal preservation conditions	Away from fault	Older splay of main fault, hanging wall faults	Veins and void fills

Figures and Captions

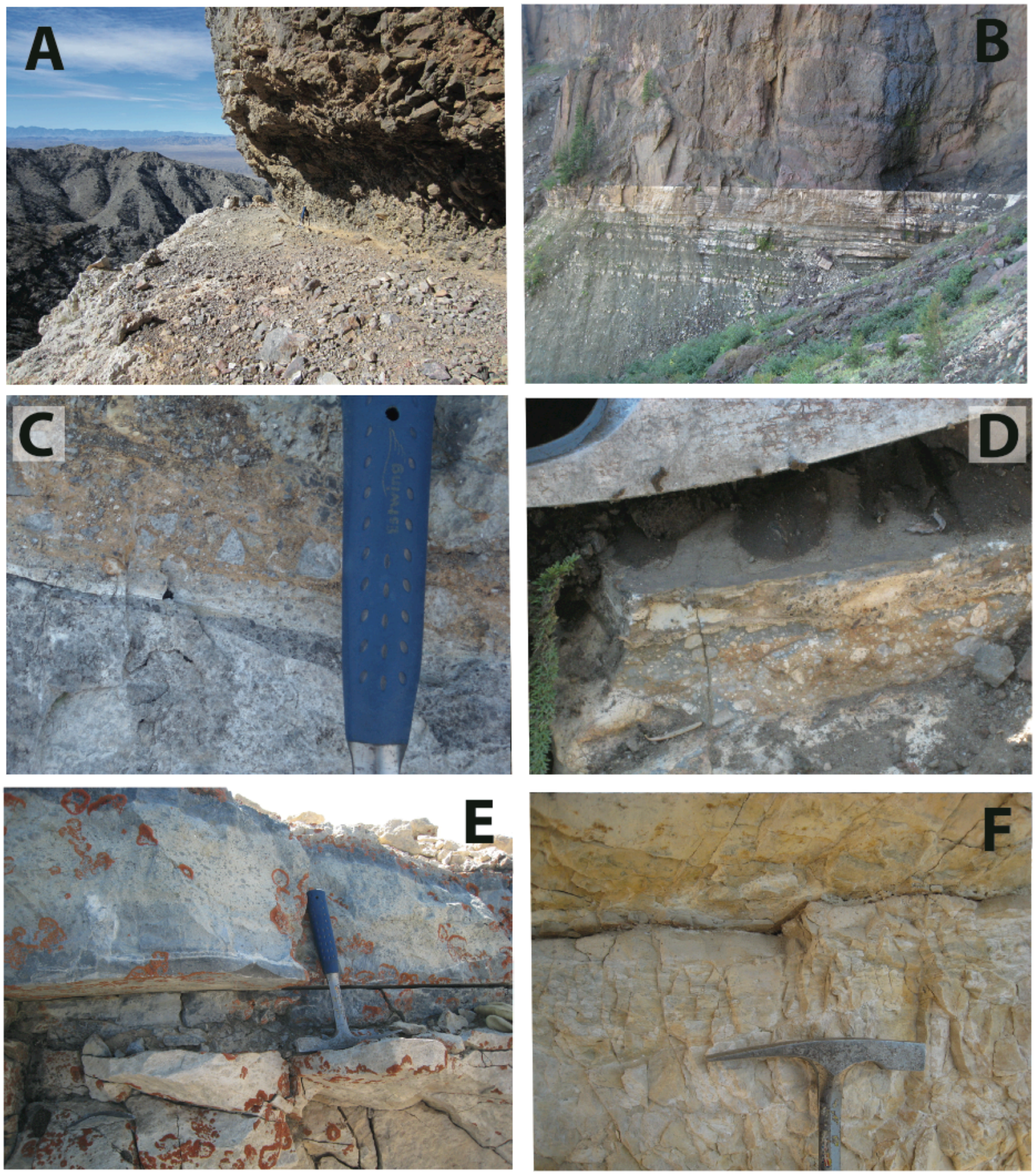

Figure 1. Photographs of fault rocks. (a), an exposure of the Mormon Peak detachment, showing preferential erosion of the brecciated hanging wall. Thin light brown detachment plane is about 2 meters below the top of the shadow. (b), an exposure of the Heart Mountain detachment, with ~35 m volcanics visible in the hanging wall in the center of frame. (c), photo of the breccia along the Mormon Peak detachment (DET-b), with the main slip surface at the top of the dark gray wedge. (d), photo of breccia along the Heart Mountain detachment (DET-b), with the dark shadowed surface containing veneers of hanging wall over the top of the breccia. (e), photo of a hanging wall fault breccia at Heart Mountain (HW-f). (f), photo of hanging wall fault breccia at Steamboat, Heart Mountain detachment.

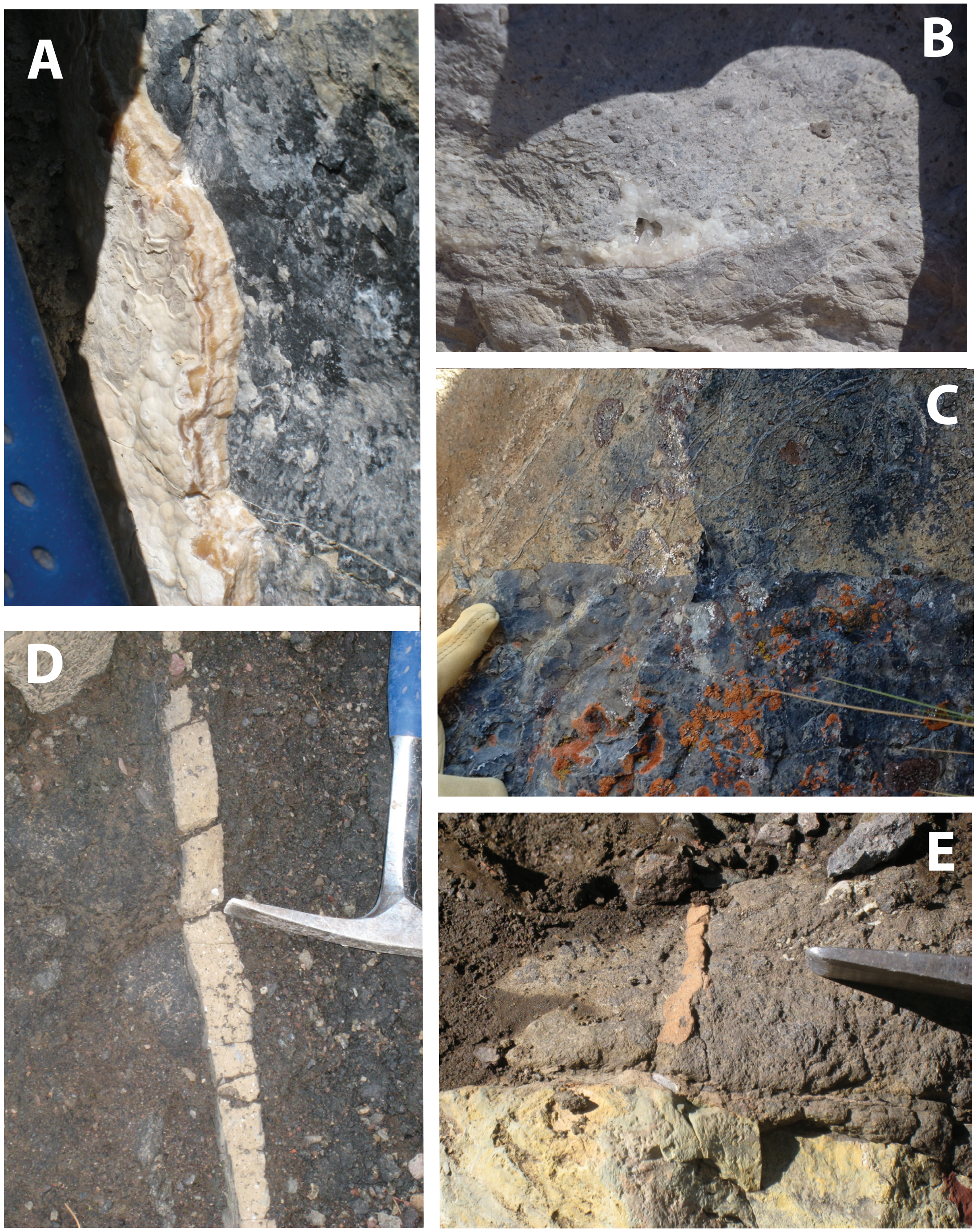

Figure 2. Photographs of sample types: (a), hanging wall vein (HW-v), about 1 cm in width; (b), hanging wall void fill (HW-v) from Heart Mountain, with calcite spar filling an irregular void in a breccia; (c), the basal layer breccia at White Mountain, where the hanging wall is metamorphosed to marble (DET-m); (d), clastic dike (HW-c) from Jim Smith Creek; (e), smaller clastic dike (HW-c) just above the detachment (base of dark gray volcanic hanging wall), but not continuous with it within the plane of the photo.

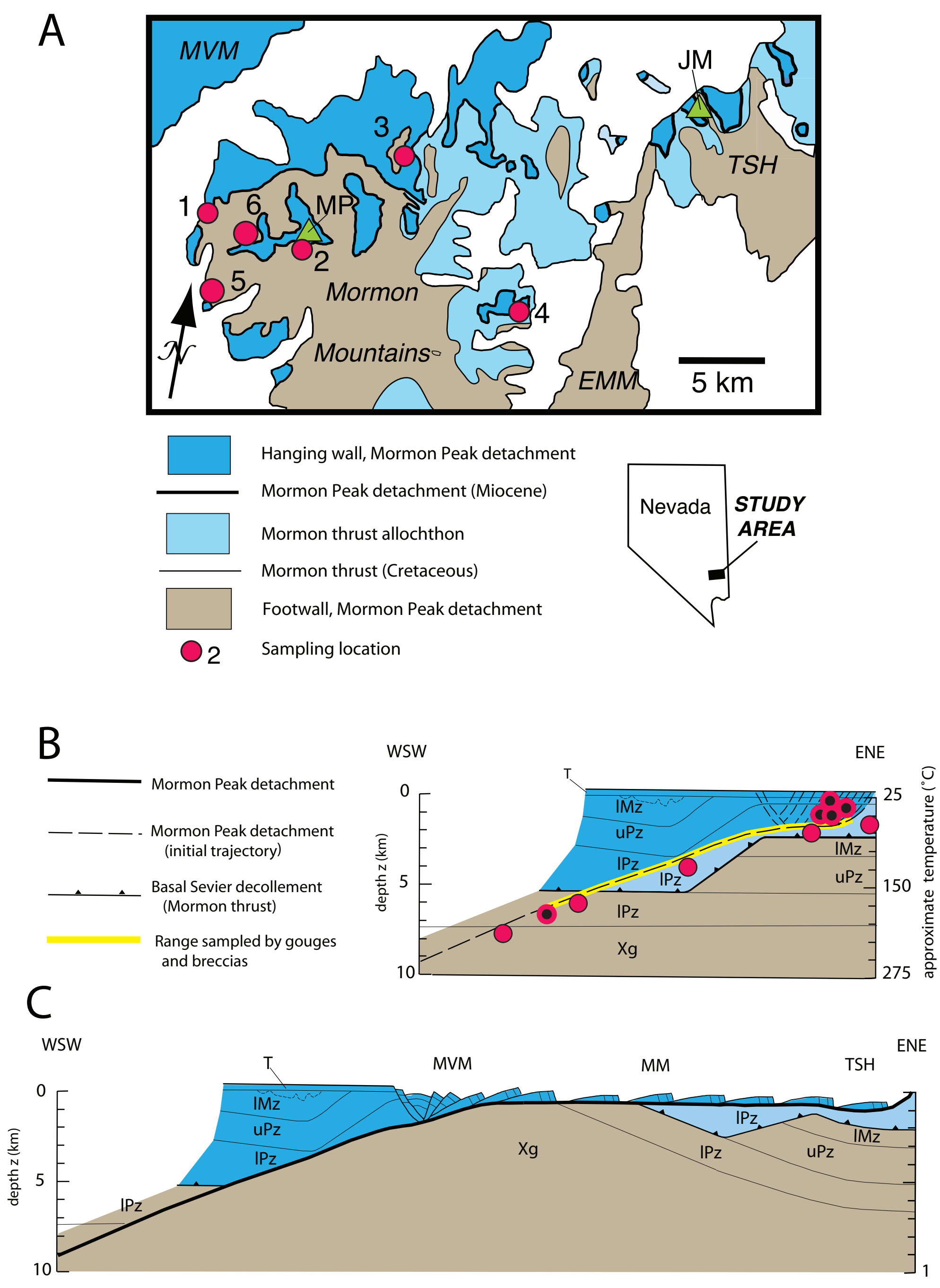

Figure 3. Structural map and schematic cross-section of the Mormon Mountains, Nevada. (a), map showing the sample locations. MVM, Meadow Valley Mountain; MP, Mormon Peak; JM, Jumbled Mountain; TSH, Tule Spring Hills; EMM, East Mormon Mountains. (b), reconstructed cross-section. Xg, pre-Cambrian basement; lPz, Cambrian-Mississippian strata; uPz, Pennsylvanian and Permian strata; lMz, Triassic through Jurassic strata; T, Tertiary volcanic strata. (c), post-detachment geometry.

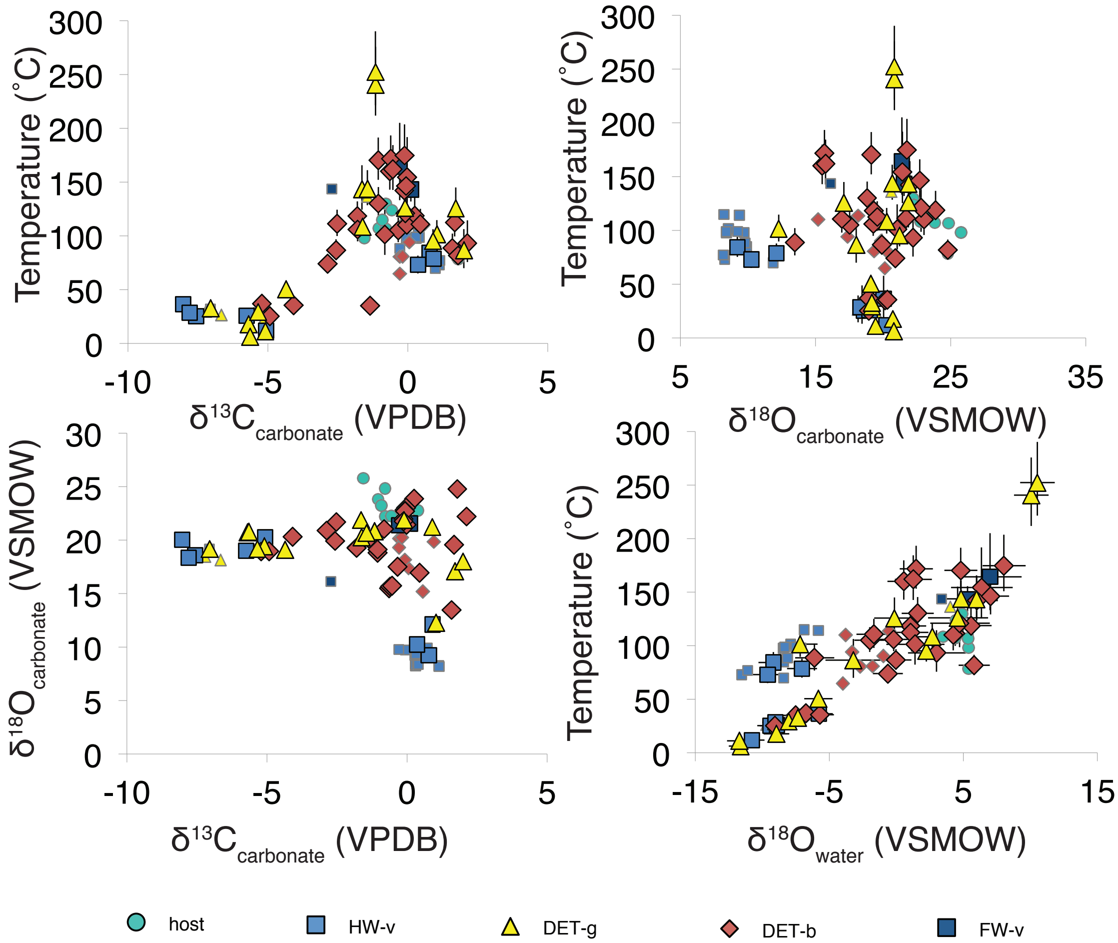

Figure 4. Isotopic data for samples from the Mormon Mountains, Nevada, keyed by texture. Errors are 1-sigma standard errors, and smaller than the symbol size for $\delta^{18}O_{carbonate}$ and $\delta^{13}C$ analyses. Smaller symbols indicate data previously published in Swanson et al., 2012.

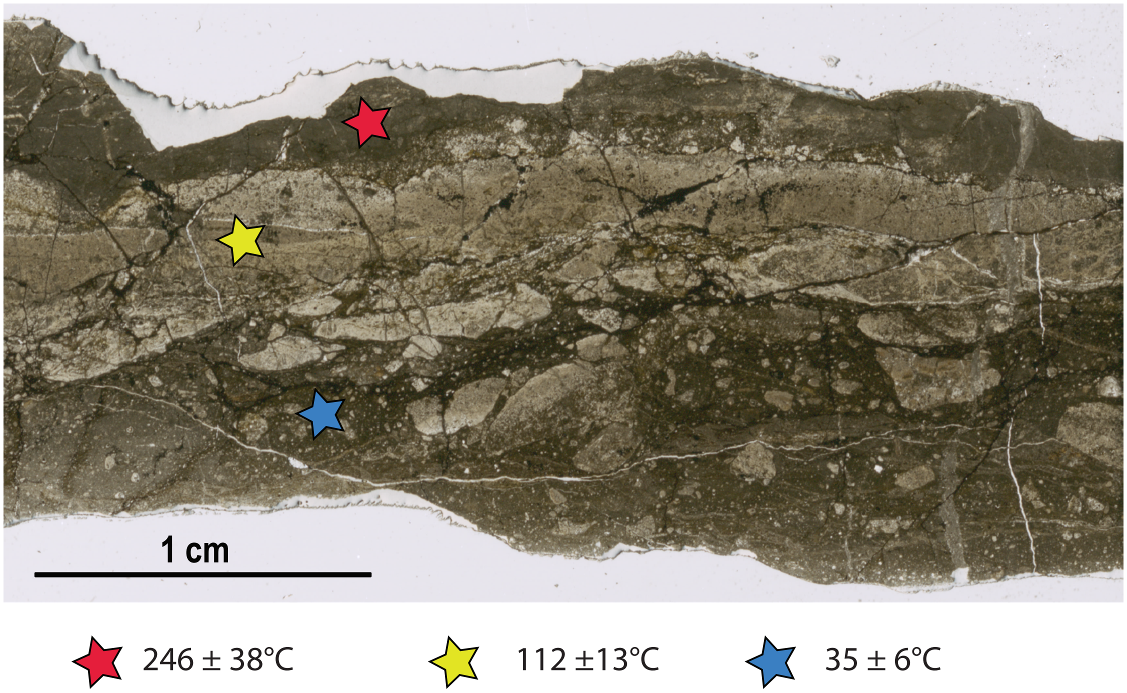

Figure 5. Thin section scan of sample ES10-23, showing the 3 layers with distinct textures and temperatures.

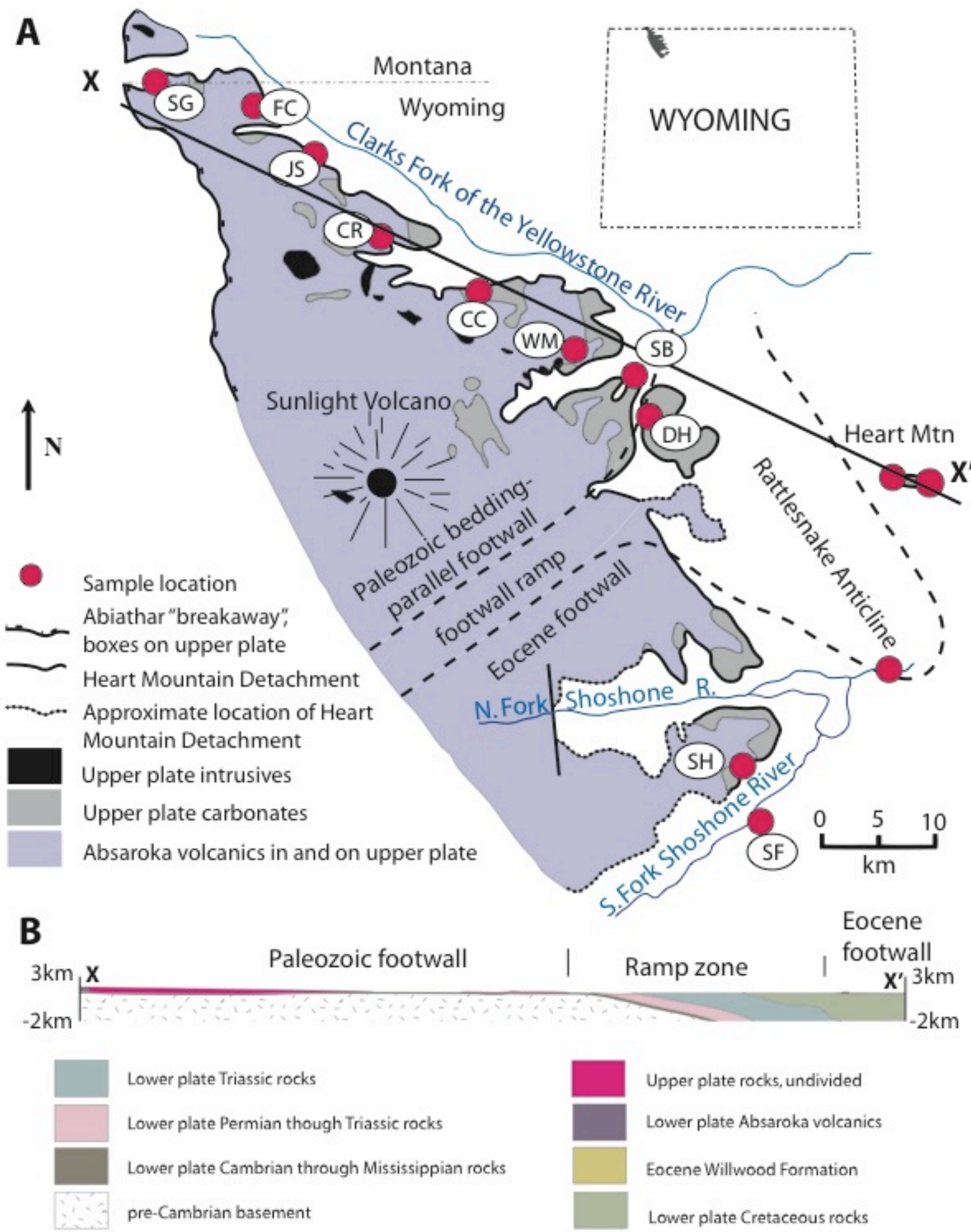

Figure 6. (a) Map and (b) 1:1 cross-section of the Heart Mountain allochthon. SG, Silvergate; FC, Fox Creek; JS, Jim Smith Creek; CR, Crandall Creek; CC, Cathedral Cliffs; WM, White Mountain; SB, Steamboat; DH, Dead Indian Hill; SH, Sheep Mountain; SF, South Fork of the Shoshone River.

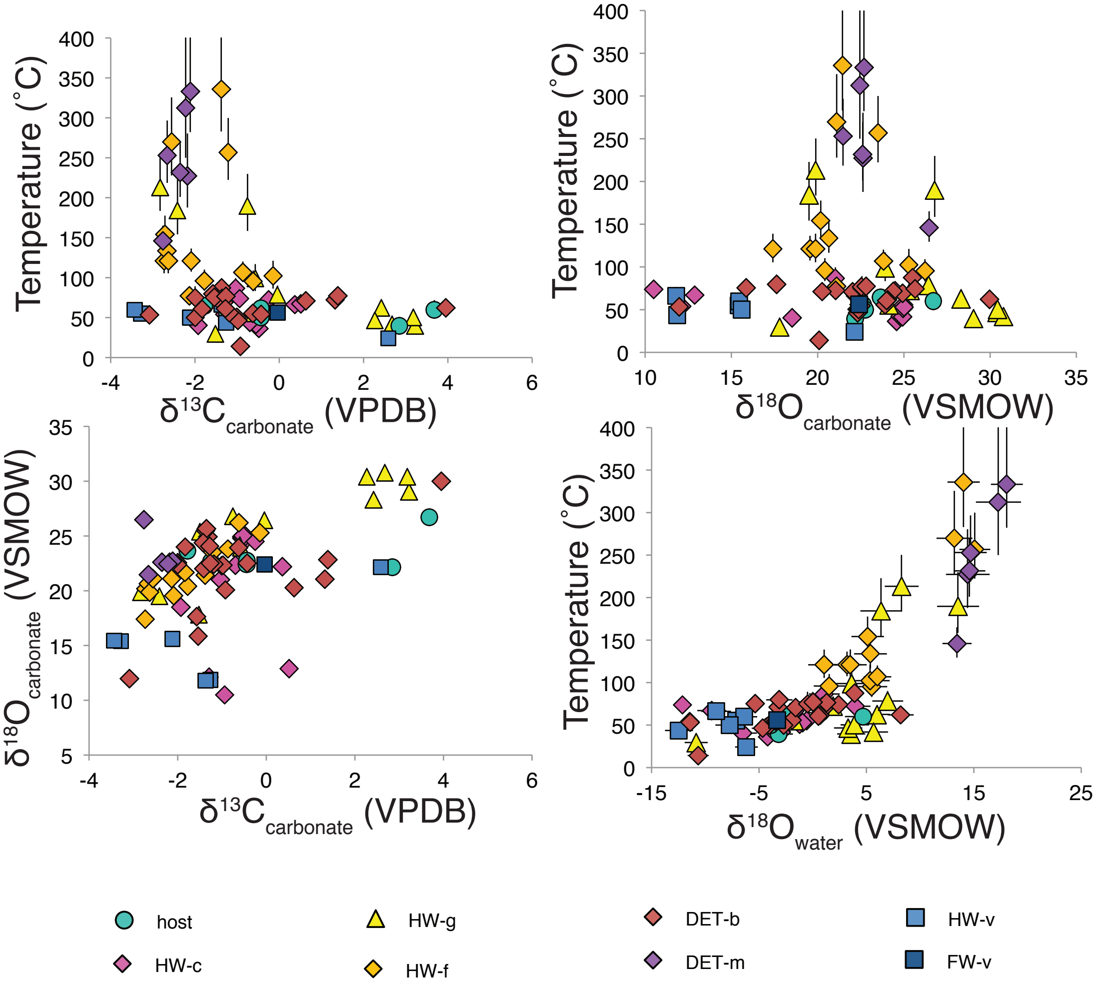

Figure 7. Isotopic data for samples from near the Heart Mountain allochthon, Wyoming, keyed by texture. Errors are 1-sigma standard errors, and smaller than the symbol size for $\delta^{18}O_{carbonate}$ and $\delta^{13}C$ analyses.

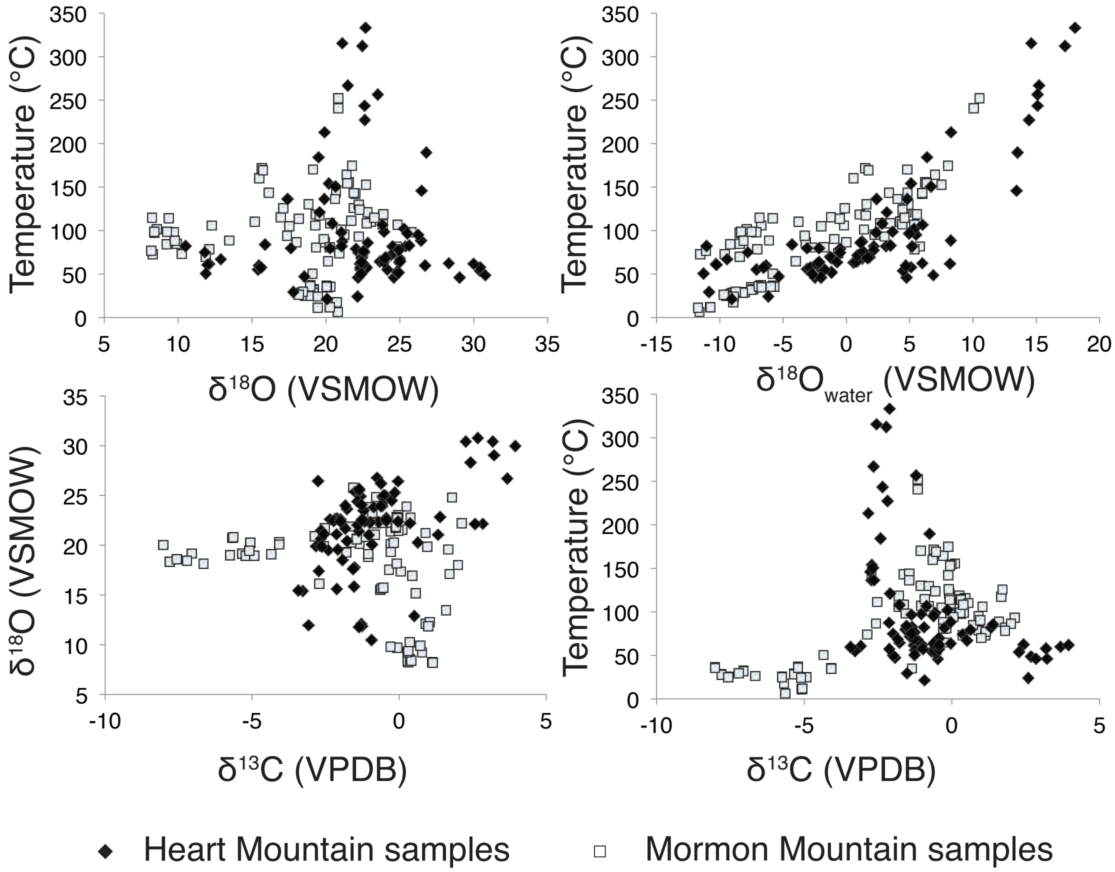

Figure 8. Isotopic data, keyed by detachment fault area

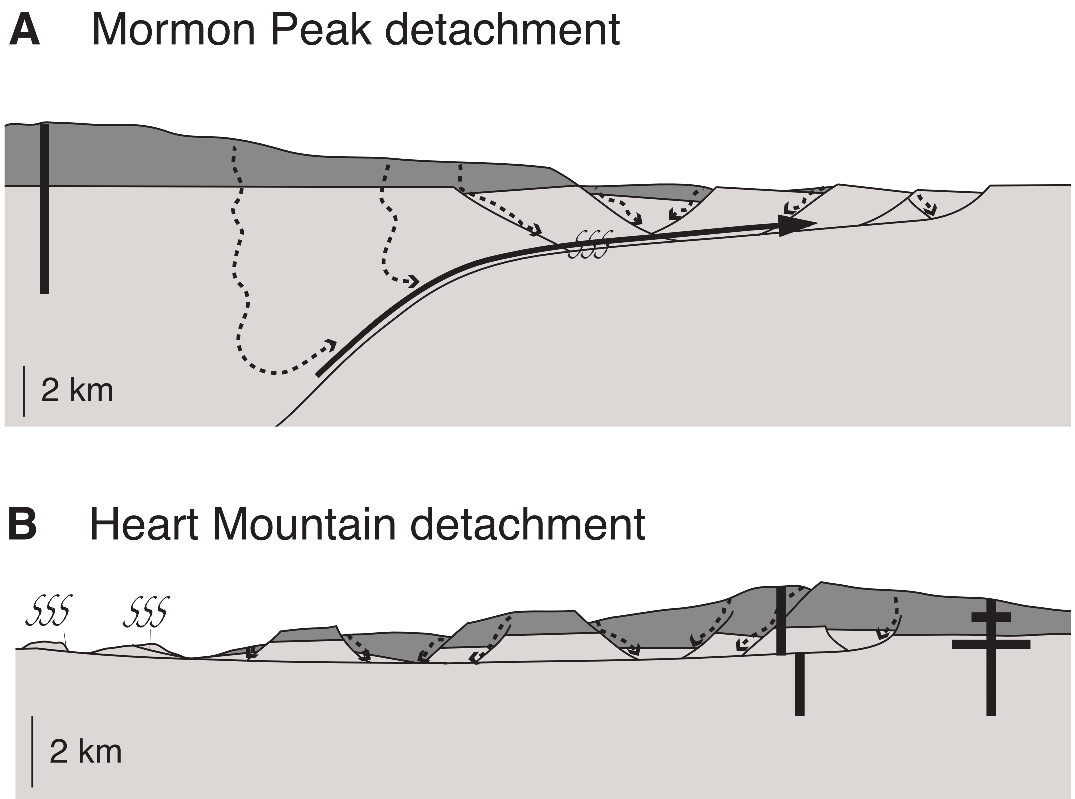

Figure 9. Schematic diagram summarizing comparison between (a) Mormon Peak and (b) Heart Mountain isotopic results. Dashed, wavy lines with arrows, infiltration of meteoric water; solid line with arrow, up-dip migration of meteoric fluid; "s"-pattern, shear heating on detachment and hanging wall faults; heavy vertical and horizontal lines, volcanic source regions; dark gray, Tertiary volcanics; light gray, Precambrian/Paleozoic substrate.